Journal of ELECTRONIC MATERIALS, Vol. 46, No. 7, 2017
DOI: 10.1007/s11664-017-5321-3

Influence of CoO Nanoparticles on Properties of Barium Zirconium Titanate Ceramics

PARKPOOM JARUPOOM,[1] PHARATREE JAITA,[2,3] NARONGDETCH BOOTHRAWONG,[2] THANATEP PHATUNGTHANE,[4] RATABONGKOT SANJOOM,[5] GOBWUTE RUJIJANAGUL,[2,7] and DAVID P. CANN[6]

1.—Department of Industrial Engineering, Faculty of Engineering, Rajamangala University of Technology Lanna, Chiang Mai 50300, Thailand. 2.—Department of Physics and Materials Science, Faculty of Science, Chiang Mai University, Chiang Mai 50200, Thailand. 3.—Science and Technology Research Institute, Chiang Mai University, Chiang Mai 50200, Thailand. 4.—Division of Science, Faculty of Education, Nakhon Phanom University, Nakhon Phanom 48000, Thailand. 5.—Department of Applied Science and Biotechnology, Faculty of Agro-Industrial Technology, Rajamangala University of Technology Tawan-ok Chanthaburi Campus, Chanthaburi 22210, Thailand. 6.—Materials Science, School of Mechanical, Industrial, and Manufacturing Engineering, Oregon State University, Corvallis, OR 97331, USA. 7.—e-mail: rujijanagul@yahoo.com

Composites of $Ba(Zr_{0.07}Ti_{0.93})O_3$ ceramic and CoO nanoparticles (at 1.0 vol.% to 3.0 vol.%) have been fabricated to investigate the effects of the CoO nanoparticles on the properties of the composites. X-ray diffraction data revealed that the modified samples contained $Ba(Zr_{0.07}Ti_{0.93})O_3$ and CoO phases. Addition of CoO nanoparticles improved the magnetic behavior and resulted in slight changes in ferroelectric properties. The composites showed a magnetoelectric effect in which the negative value of the magnetocapacitance increased with increasing CoO concentration. Examination of the dielectric spectra showed that the two phase-transition temperatures as observed for unmodified $Ba(Zr_{0.07}Ti_{0.93})O_3$ merged into a single phase-transition temperature for the composite samples. The composite samples also showed broad relative permittivity versus temperature (ε_r–T) curves with frequency dispersion. This dielectric behavior can be explained in terms of the Maxwell–Wagner mechanism. In addition, the Vickers hardness (H_v) value of the samples increased with increasing CoO content.

Key words: Magnetic properties, mechanical properties, x-ray diffraction, electrical properties

INTRODUCTION

Barium titanate ($BaTiO_3$, BT) with perovskite structure has been widely investigated because of its good dielectric and excellent ferroelectric properties.[1] The properties of BT can be efficiently controlled by doping with different elements. It has been reported that modified BT ceramics, e.g., with zirconium (Zr) doped at titanium (Ti) site, i.e., $Ba(Zr_xTi_{1-x})O_3$ (BZTs), show improved electrical properties.[1–3] Many authors have reported that the properties of BZTs are dependent on the Zr concentration; For example, BZTs present three phase transitions, i.e., rhombohedral to orthorhombic (T_1), orthorhombic to tetragonal (T_2), and tetragonal to cubic (T_c), at temperatures that depend strongly on the Zr concentration. High dielectric constant (~12,000 at $T_c \approx 105°C$) with low loss tangent ($\tan\delta \approx 0.035$) was observed for $Ba(Zr_{0.07}Ti_{0.93})O_3$ ceramic.[4] High dielectric tunability has also been reported for some BZT compositions.[5,6] Furthermore, $Ba(Zr_{0.07}Ti_{0.93})O_3$ doped with B_2O_3 presented very high strain under applied electric fields,[7] and $Ba(Zr_{0.2}Ti_{0.8})O_3$–$(Ba_{0.7}Ca_{0.3})TiO_3$ doped with praseodymium (Pr) showed

(Received June 20, 2016; accepted January 17, 2017; published online February 27, 2017)

luminescence properties.[8] Therefore, BZT-based ceramics are very attractive materials for use in many electronic applications.[4–9]

For many years, researchers have attempted to create novel materials which exhibit both ferroelectric and magnetic properties in one system.[10] Such materials are called multiferroic materials. However, a single phase or solid solutions of many multiferroic materials exhibit weak ferroelectric and/or magnetic properties.[11,12] Therefore, many researchers have tried to find new materials having stronger multiferroic properties. An alternative approach to obtain strong multiferroic properties is to produce composites or nanocomposites[13–16] which contain ferroelectric and magnetic phases.[16,17] This composite approach has been applied to produce many multiferroic composites, such as $La_{0.7}Ba_{0.3}MnO_3/BaTiO_3$,[18] $Ba(Zr_{0.07}Ti_{0.93})O_3/NiO$,[19] $Na_{0.5}Bi_{0.5}TiO_3/MnFe_2O_4$,[20] and $Pb(Zr_{0.52}Ti_{0.48})O_3/CoFe_2O_4$.[21]

In the present work, new $Ba(Zr_{0.07}Ti_{0.93})O_3$/CoO (BZT/CoO) composites were fabricated and their properties investigated, since BZT presents many interesting properties and CoO is a magnetic material. In this work, CoO nanoparticles were added to BZT to form the ceramics. Many characteristics of the composites, including their dielectric, ferroelectric, and magnetic properties, were investigated and are discussed in detail. They were also characterized, particularly in terms of density, phase formation, and microstructural and mechanical properties, and the corresponding results are also presented herein.

EXPERIMENTAL PROCEDURES

In this work, reagent-grade oxide powders of $BaCO_3$, ZrO_2, and TiO_2 were used as starting materials, weighed based on the stoichiometric formula $Ba(Zr_{0.07}Ti_{0.93})O_3$ (BZT). The weighed batch was ball-milled for 24 h. The mixed powder was then calcined at 1200°C for 2 h. Nanoparticulate CoO powder (Sigma-Aldrich), with particle size <100 nm, was used for the nanocomposites. Different volume ratios of CoO nanoparticles (0 vol.%, 1 vol.%, 2 vol.%, and 3 vol.%) were ultrasonically dispersed in ethanol for 30 min before mixing with BZT powder and milling for 24 h. The resulting slurries were then dried for 24 h. The obtained powders were pressed into disc-shaped pellets. These green pellets were sintered at temperatures ranging from 1150°C to 1500°C for 2 h. The phase formation in the ceramics and composites was determined by x-ray diffraction (XRD) analysis. The bulk density of the sintered samples was measured by Archimedes' method. Microstructural study of the sintered samples was performed by scanning electron microscopy (SEM, JEOL JSM-6335F). Grain size was determined by the mean linear intercept method on SEM micrographs.

For electrical measurements, samples were polished to obtain very smooth and parallel surfaces, and silver paste was painted on both sides of the samples and fired at 650°C for 30 min. The dielectric properties of the ceramics were studied using an *LCR* meter connected to a high-temperature furnace at frequencies ranging from 20 Hz–2.25×10^6 Hz. Polarization–electric field (*P*–*E*) hysteresis loops were measured at RT using a ferroelectric test system from Radiant Technologies. An alternating-current (AC) electric field of 20 kV/cm and frequency of 1 Hz were used in these measurements. The magnetic properties of the composites were measured using a vibrating-sample magnetometer (VSM) (model 7404, Lake Shore Cryotronics, Inc., Westerville, OH, USA). Vickers hardness (H_v) was measured on a polished surface using a microhardness tester, to study the mechanical properties.

RESULTS AND DISCUSSION

Densification and Phase Formation

To achieve optimum densification, samples were sintered at different temperatures from 1150°C to 1500°C. The density of the samples sintered at different temperatures is shown in Fig. 1a. These density data reveal that the concentration of the nanoparticles and the sintering temperature both affected the sintered density. For the pure BZT sample, the highest density was obtained when sintered at 1450°C (Fig. 1a, inset). For the composite samples, the density increased with increasing sintering temperature and showed a maximum value at 1250°C, decreasing slightly thereafter. Plots of the optimum density and its optimum sintering temperature as a function of CoO content are shown in Fig. 1b. The porosity of the samples also reduced with the additive (Fig. 1b, inset). The optimum sintering temperature decreased from 1450°C for the pure BZT sample to 1250°C for the composite samples. Therefore, the optimum sintering temperature for the composites was 200°C lower compared with that of the pure BZT sample. Furthermore, the density increased with the CoO content at the optimum sintering temperature. The densest sintered samples for each composition were selected for characterization.

Figure 2 displays x-ray diffraction (XRD) patterns with $2\theta = 20°$ to 80° for all the samples at room temperature (RT). All of the main diffraction peaks correspond to perovskite structure. Although there are conflicting data regarding the symmetry of BZT ceramics,[22,23] the present XRD data match with International Centre for Diffraction Data (ICDD) file no. 01-081-2198, and the symmetry of the samples was characterized as orthorhombic. The XRD data also showed CoO phase (ICDD file no. 01-071-1178, indicated by "*"), which is a magnetic material.[24] Furthermore, the intensity of the CoO peaks increased with increasing amount of additive. This result reveals that the modified samples are a kind of composite. It should be noted that the XRD

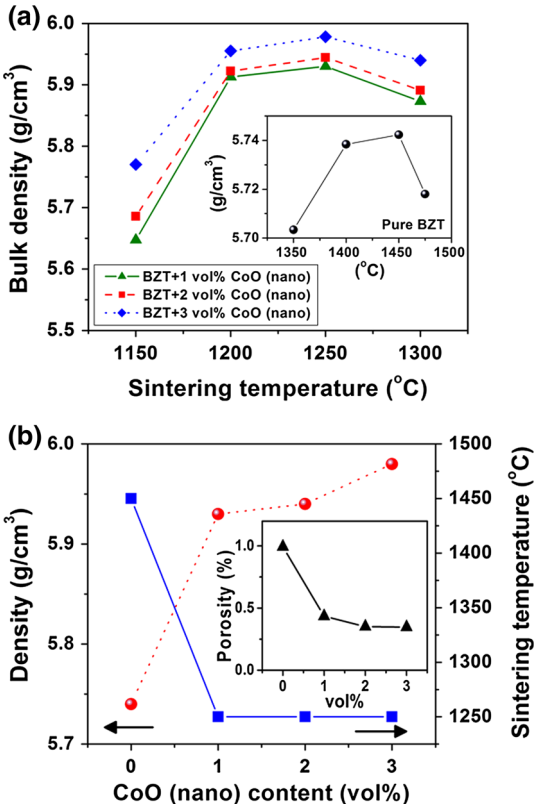

Fig. 1. (a) Variation of bulk density with sintering temperature for the composites (inset: density for pure BZT ceramic), (b) optimum density and corresponding sintering temperature as a function of the CoO content of the BZT/CoO composites (inset: porosity versus CoO concentration).

peaks shifted to lower angle, indicating distortion of the unit cell. This may be due to some Co ions entering the BZT lattice. To check the effect of CoO additive on the phase formation in more detail, the Raman scattering technique was employed. Composition-dependent Raman spectra for the studied samples are illustrated in Fig. 3. For the pure BZT sample, the Raman spectrum agrees with data from many previous works.[22,25] The Raman spectra present E(TO_1) and E1(TO_2) modes at approximately 110 cm^{-1} and 300 cm^{-1}, which can be linked with the tetragonal–cubic phase transition.[25,26] The stretching mode of $A_1(TO_1)$ and $A_1(TO_3)$ were observed at approximately 166 cm^{-1} and 516 cm^{-1}, respectively.[22,25,26] Furthermore, there was a coupling between the sharp $A_1(TO_1)$ and broad $A_1(TO_2)$ modes.[22] $A_1(LO_3)$ mode was found at 710 cm^{-1}, where its intensity can be associated with zirconium (Zr) substitution at titanium (Ti) sites at the B-site of the BZT lattice.[22] After adding the nanoparticles, obvious change of the Raman spectra was observed; i.e., some fine features shifted or disappeared. Broader main peaks were found for the composite samples, suggesting structural disturbance of the present composites due to the CoO additive.

Ferroelectric and Magnetic Properties

The *P–E* hysteresis loops obtained at room temperature for the samples with different CoO contents are shown in Fig. 4. The pure BZT sample showed normal ferroelectric behavior with a nearly rectangular hysteresis loop. The ferroelectric properties of the pure BZT sample are close to those in previous literature.[9] However, the composite samples presented unsaturated hysteresis loops that became more slanted. The remanent polarization (P_r) versus CoO content is illustrated in Fig. 5. The P_r value tended to decrease with increasing CoO content. The sample with 2.0 vol.% CoO showed the highest P_r value of 12.5 $\mu C/cm^2$, compared with the other composite samples. To quantify the changes in the hysteresis, the squareness (R_{sq}) of the hysteresis loops was determined from the equation: $R_{sq} = (P_r/P_s) + (P_{1.1E_c}/P_r)$,[9,27] where P_s is the saturated polarization and E_c is the coercive field. The R_{sq} values versus CoO content are illustrated in the inset of Fig. 5. The R_{sq} value tended to decrease with increasing CoO content. However, the R_{sq} value for the 1 vol.% sample ($R_{sq} = 0.78$) was close to that of the 2 vol.% sample ($R_{sq} = 0.79$), suggesting that the quantified hysteresis loop behavior of these samples changed only slightly between the 1 vol.% and 2 vol.% composites.

The magnetization–magnetic field (*M–H*) plots obtained at RT for the studied samples are illustrated in Fig. 6, showing square hysteresis loops with M_r increasing from 0 emu/g for the pure BZT sample to 2.4 emu/g for the 3 vol.% sample (Fig. 5). In the present work, the magnetic moment (n_B) of the ceramics was determined in units of the Bohr magneton (μ_B) using the equation: $n_B = (M \times \sigma'_S)/5585$, where M is the molecular weight of the particular composition, σ'_S represents the magnetization/gram (emu/gram) of the sample, and 5585 is the magnetic constant. The value of n_B increased with increasing CoO content (Fig. 7, inset). This result agrees well with many previous works on multiferroic composites; i.e., n_B increased with increasing amount of magnetic phase.[21,28] However, it should be noted that the n_B values in the present work showed a nonlinear relation with the amount of additive. This is probably due to entry of some Co ions into the BZT lattice, so the studied samples contained not only BZT and CoO but also Co-doped BZT phase (i.e., the modified samples were multiphase). The observation of ferromagnetic behavior for the studied ceramics may be due to the effect of particle size, as nanoparticles of many antiferromagnetic materials present ferromagnetic behavior.[24,29] Recently, the F-center exchange mechanism[30–33] has been used to explain an improvement in the ferromagnetic behavior of many materials, e.g., Fe-doped SnO_2 thin films[34] and Fe-doped $Bi_4Ti_3O_{12}$.[33] When Fe is doped into such materials, Fe^{3+}-□-Fe^{3+} groups (where -□- represents an oxygen vacancy) can be formed in the structure. An electron trapped in the oxygen vacancy can produce an F-center, where the

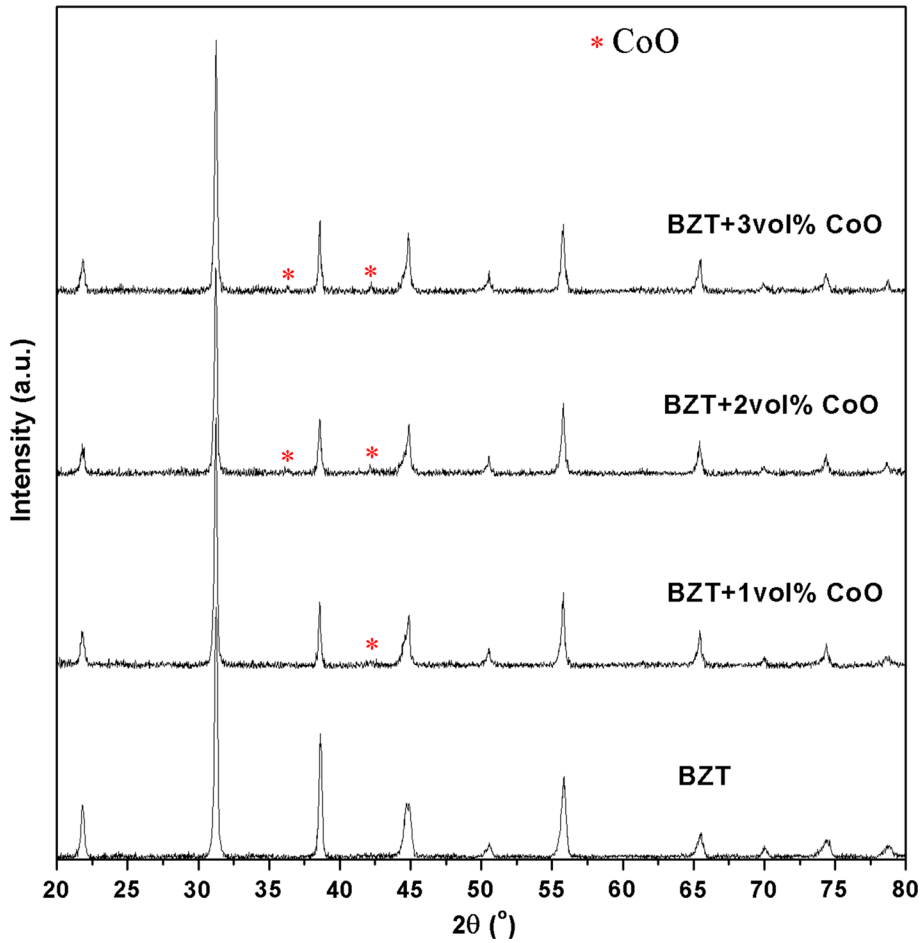

Fig. 2. X-ray diffraction patterns at 2θ = 20° to 80° for pure BZT and BZT/CoO samples sintered at their optimum sintering temperature.

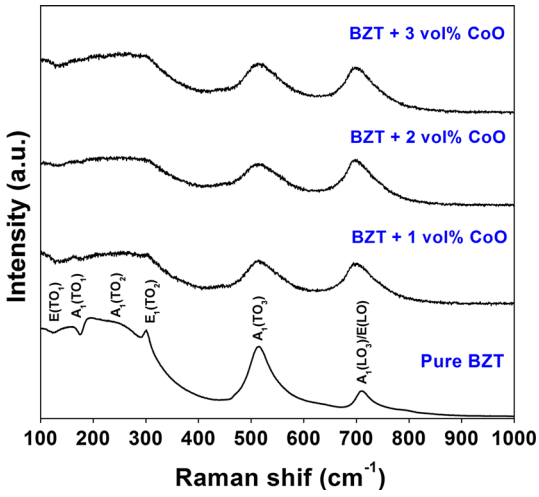

Fig. 3. Raman spectra of BZT/CoO samples with different CoO contents at RT.

trapped electron will be spin down and the two iron neighbors spin up. This leads to direct ferromagnetic coupling due to the exchange interaction of the ferric ions through the electron trapped in the bridging oxygen vacancy. This mechanism has also been used to explain the ferromagnetic behavior of $Bi_{4-x}Pr_xTi_{3-x}Co_xO_{12\pm d}$ $(0 \le x \le 0.3)$ ceramics by Yang et al.[30] They suggested that Co^{3+}-□-Co^{3+}, Co^{3+}-O-Co^{2+}, and Co^{3+}-O-Co^{3+} networks could be formed in the samples, resulting in the ferromagnetic behavior. In the present work, the improvement of the ferromagnetic behavior for the studied samples may also be linked to such an F-center exchange mechanism as reported by previous works. However, further study is required to confirm the reasons in more detail.

In the present work, the magnetoelectric (ME) effect was also studied by measuring the magnetocapacitance (indirect method). The magnetocapacitance (MC) at 1 kHz and RT was determined using the following equation: $MC\% = [(\varepsilon(H) - \varepsilon(0))/\varepsilon(0)] \times 100\%$, where $\varepsilon(0)$ is the relative permittivity at zero applied magnetic field and $\varepsilon(H)$ is the relative permittivity under an applied magnetic field (1 T). A plot of the MC value as a function of CoO concentration is presented in Fig. 7. The negative MC value increased with increasing CoO concentration. The change in relative permittivity under an external applied magnetic field suggests that there was ME coupling in the composites. This may arise from magnetic–mechanical–electric interaction between magnetostrictive

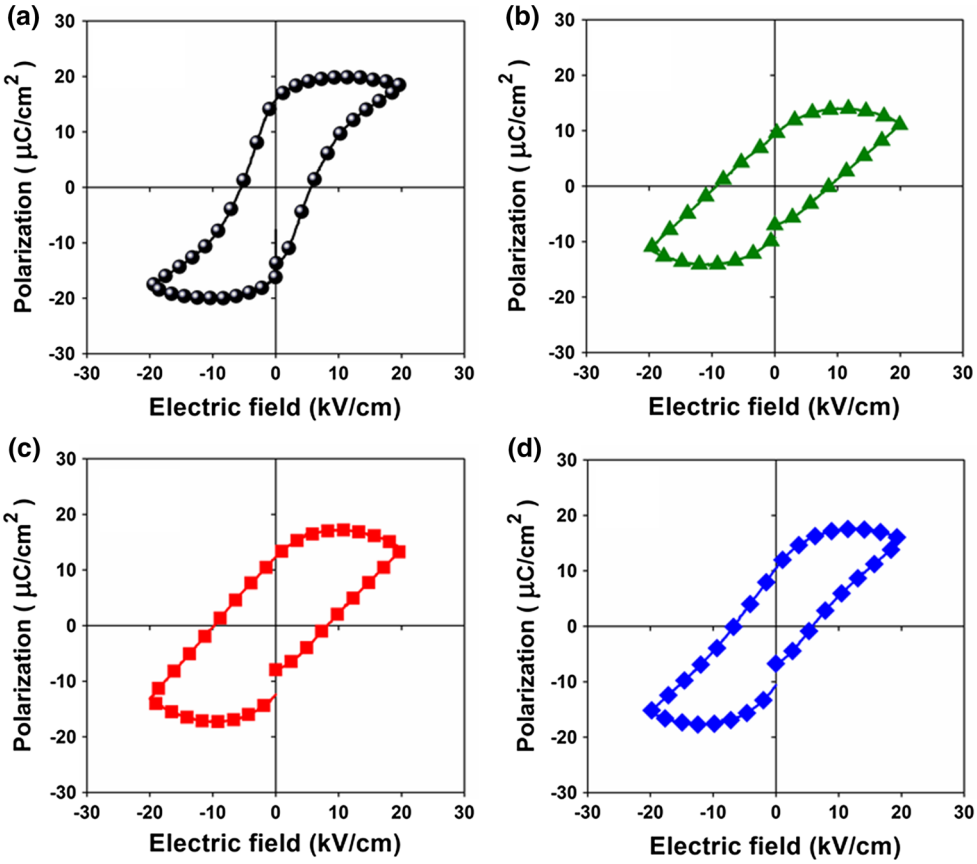

Fig. 4. *P–E* hysteresis loops for: (a) BZT, (b) BZT + 1.0 vol.% CoO, (c) BZT + 2.0 vol.% CoO, and (d) BZT + 3.0 vol.% CoO samples.

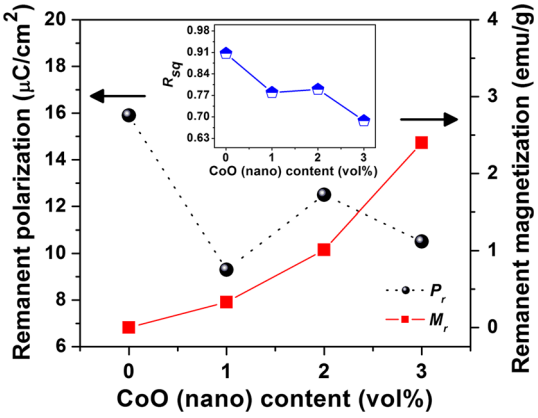

Fig. 5. Remanent polarization and remanent magnetization of ceramics (inset: R_{sq} as function of CoO content).

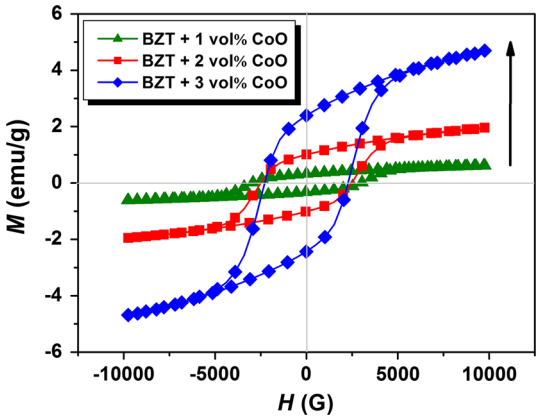

Fig. 6. Magnetization (*M*) versus magnetic field (*H*) for the ceramics.

and piezoelectric phase through the stress/strain at interfaces. In this case, the applied magnetic field can generate stress on the magnetic phase, which is transferred to the ferroelectric phase mechanically, resulting in electric polarization in the piezoelectric phase.[35,36] Kimura et al.[37] studied the ME effect in $BiMnO_3$ ceramic by using a potential in thermodynamic theory. Normally, the potential ($\emptyset$) for a ferroelectromagnet can be expressed as[37] $\emptyset = \emptyset_0 + \alpha P^2 + \frac{\beta}{2}P^4 - PE + \alpha' M^2 + \frac{\beta'}{2}M^4 - MH + \gamma P^2 M^2$, where $\emptyset$, α, β, α', and γ are functions of temperature, and P and M are the polarization and magnetization, respectively. The term $\gamma P^2 M^2$ in this equation indicates the coupling between P and M as suggested by Kimura et al.[37] found that $\Delta\varepsilon \sim \gamma M^2$, i.e., the change in relative permittivity ($\Delta\varepsilon$) depends on the magnetization. This expression has also been used to explain the ME effect in multiferroic composites such as $x CoFe_2O_4$–$(1-x)[0.5Ba(Zr_{0.2}Ti_{0.8})O_3$–$0.5(Ba_{0.7}C_{0.3})TiO_3]$[35] and $BiFeO_3$–$CoFe_2O_4$–

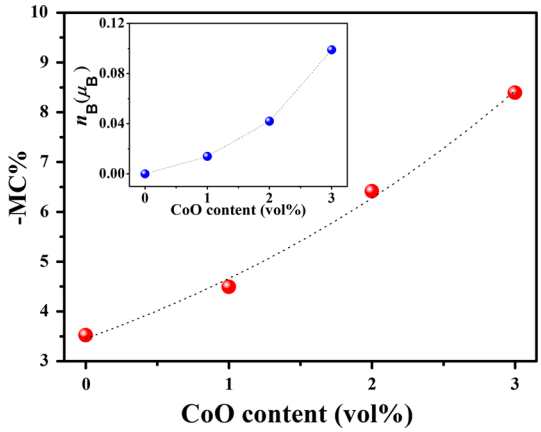

Fig. 7. –MC versus CoO content [inset: Bohr magneton (n_B) as function of CoO content].

$PbTiO_3$.[38] Thus, the change in relative permittivity (or the presence of the ME effect) in the present work may be understood using this expression.

Dielectric Properties

The relative permittivity (ε_r) as a function of temperature for the ceramics with different CoO contents is shown in Fig. 8. For the pure BZT sample, two phase transitions were observed in the permittivity curve, denoted as T_1 (~67°C) and T_c (~102°C). The relative permittivity ($\varepsilon_{r,max}$) at T_c and at T_1 (at 1 kHz) was 12,300 and 4500, respectively. Furthermore, the pure BZT sample also showed very weak frequency dependence of the relative permittivity. These properties are consistent with data reported in previous works.[39,40] For the

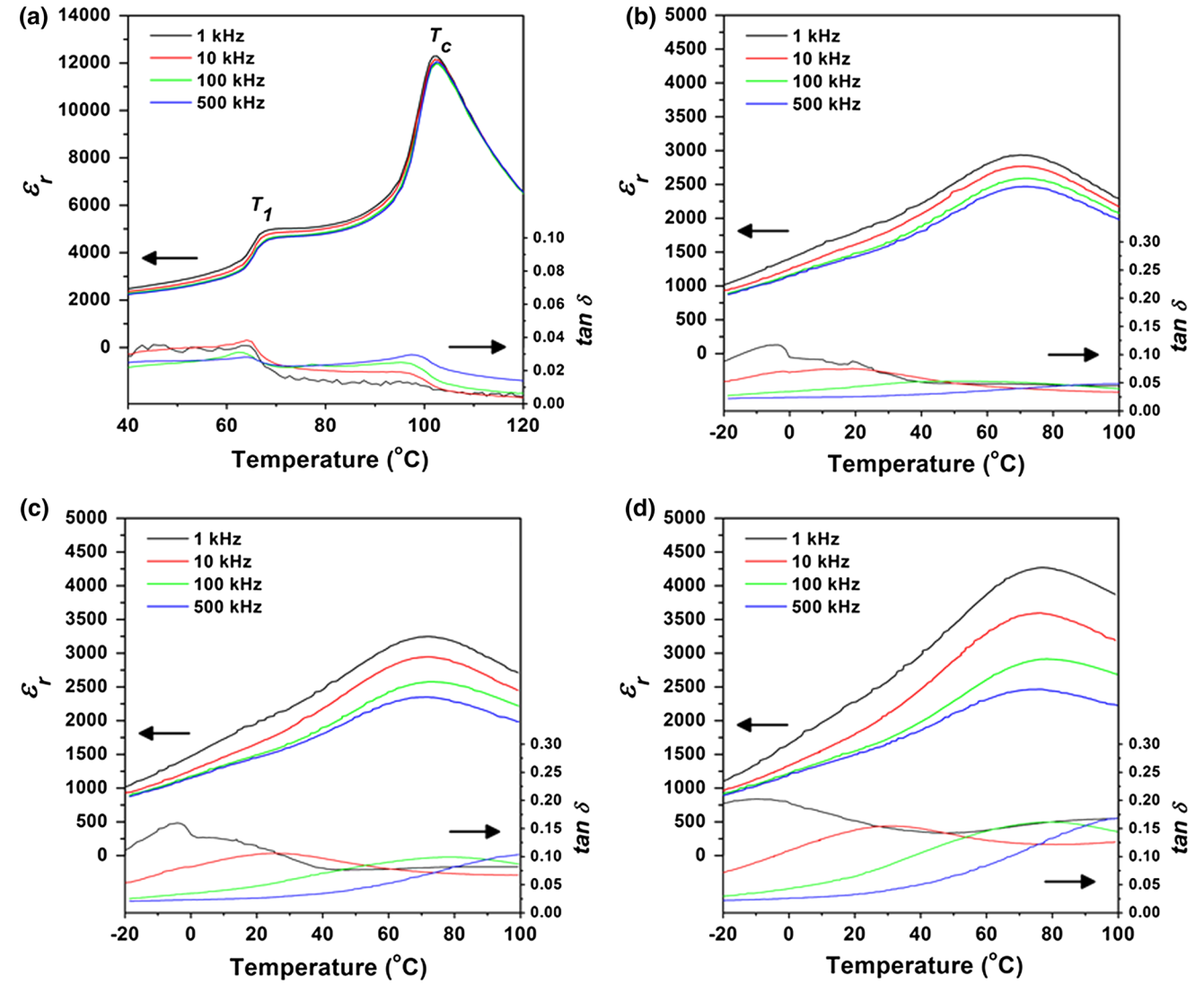

Fig. 8. Relative permittivity (ε_r) and loss tangent (tan δ) as functions of temperature and frequency for: (a) BZT, (b) BZT + 1.0 vol.% CoO, (c) BZT + 2.0 vol.% CoO, and (d) BZT + 3.0 vol.% CoO samples.

composite samples, the permittivity curves showed a single, broad phase transition. The permittivity curves of the composites also displayed pronounced frequency dependence. The presence of such frequency dependence of the relative permittivity with the additive may be due to the samples having more heterogeneous conduction. To check this effect, room-temperature relative permittivity versus frequency curves are plotted in Fig. 9. The relative permittivity curves for the composites presented dielectric constant steps down from high values at low frequency, while the pure BZT sample showed only a slight change in relative permittivity with frequency. It should be noted that the steps in the relative permittivity curves were clearly noted for the composites containing ≥2.0 vol.% CoO. Furthermore, the composite with 3.0 vol.% CoO presented the highest level of relative permittivity at room temperature (see also the inset of Fig. 9), especially in the low frequency region. This behavior can be explained in terms of the Maxwell–Wagner polarization mechanism due to the samples having heterogeneous conduction.[41] In this work, this may be linked to the different conduction in insulator/conductive areas and sample/electrode interfaces in the composites. Plots of the loss tangent (tan δ) versus temperature are also shown in Fig. 8. The tan δ value tended to increase with increasing amount of additive. Furthermore, samples with higher CoO content showed greater frequency dispersion of tan δ, consistent with the permittivity curves. Higher CoO content also resulted in higher value of loss tangent at low frequency.

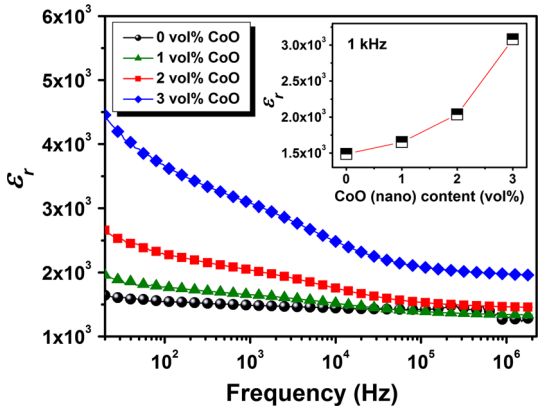

Fig. 9. Frequency dependence of relative permittivity (at RT) of the studied BZT/CoO samples (inset: ε_r at RT and 1 kHz as function of CoO content).

Microstructure and Mechanical Properties

Selected SEM micrographs and corresponding energy-dispersive x-ray spectrometry (EDS) maps (for Co) are shown in Fig. 10. The white spots in the EDS maps indicate Co. For the samples with less CoO (e.g., 1.0 vol.%), a nonuniform distribution of Co spots was noted (Fig. 10b), suggesting that the composites had heterogeneous composition. The number of Co spots increased with the amount of

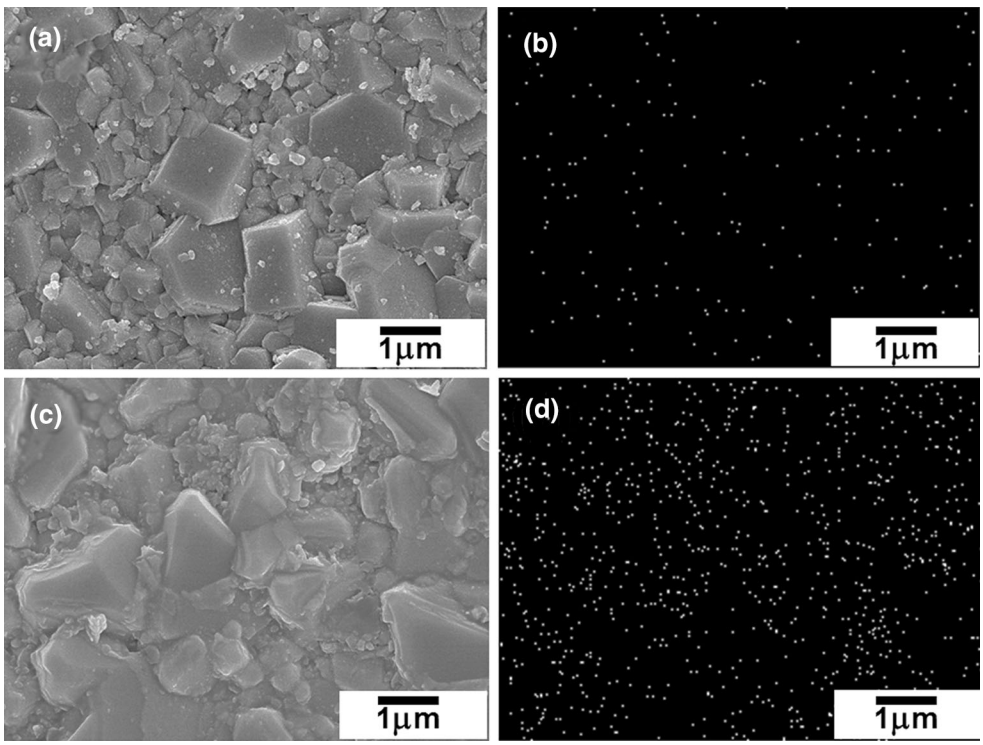

Fig. 10. Selected SEM micrographs and corresponding EDS maps of BZT + 1.0 vol.% CoO sample (a, b) and BZT + 3.0 vol.% CoO sample (c, d).

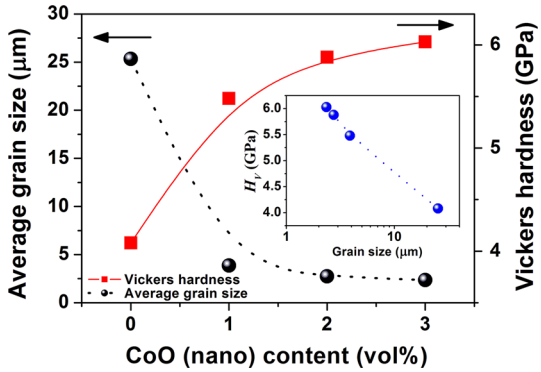

Fig. 11. Average grain size and Vickers harness as functions of CoO content for the ceramics [inset: H_v versus log(d)].

additive (Fig. 10d). Microstructural analysis also showed that addition of the additive resulted in a change in grain size. The average values of grain size, as calculated by the linear intercept method, decreased sharply from 25.3 μm for the pure BZT sample to 3.9 μm for the 1.0 vol.% sample, then slightly to 2.4 μm for the 3.0 vol.% sample (Fig. 11). Furthermore, nonuniformity in grain size was found for samples with higher CoO content (e.g., 3.0 vol.%). This reduction in grain size may be due to the additive phase preventing grain-boundary movement during the sintering process.[42]

It has been reported that the mechanical properties of many electroceramics can be improved by adding nanoparticles.[13,43,44] In the present work, H_v was investigated to study the effect of nanoparticle addition on this property. The Vickers hardness value as a function of CoO content is also displayed in Fig. 11. These results reveal that the nanoparticles improved the hardness value, from 4.1 GPa for the pure BZT sample to 6.0 GPa for the 3.0 vol.% sample. This improvement in the hardness value for the studied samples may be due to the nanoparticles physically reinforcing grain boundaries and acting as effective pins against microcrack propagation.[43] Grain size (d) is also widely known to affect the mechanical properties of many materials. Grain size and hardness are therefore often interrelated. In the case of metallic materials, the Hall–Petch equation ($H_v = H_0 + kd^{-1/2}$, where H_0 and k are constants) has been used to relate grain size and yield strength. This equation has also been used to link the grain size and hardness of some ceramics.[45,46] In the present work, however, the hardness value of the studied samples was proportional to the log of the grain size, i.e., $H_v = 6.6 - 1.9\log(d)$ (Fig. 11, inset). This suggests that the mechanical behavior of the studied composites, e.g., the hardness, differs from that of metallic materials or some ceramics, where alterations of the grain-boundary characteristics in composites can be linked to their thermomechanical behavior. Further work is required to study the grain-boundary characteristics of these composites in more detail.

CONCLUSIONS

BZT ceramics with addition of 1.0 vol.% to 3.0 vol.% CoO nanoparticles were prepared by a conventional mixed-oxide method. The properties, i.e., phase composition, microstructure, and mechanical, electrical, and magnetic properties, of the BZT/CoO nanocomposites were investigated. The results showed that the modified samples were multiphase. Addition of CoO nanoparticles enhanced the magnetic properties of the BZT ceramic with slight change in the ferroelectric properties. The additive enhanced the –MC value and had a strong effect on the phase-transition behavior of the studied samples. The composites also exhibited strong frequency dispersion of permittivity, which can be explained by the Maxwell–Wagner mechanism. In addition, the nanoparticles decreased the grain size but increased the hardness value.

ACKNOWLEDGEMENTS

The authors would like to acknowledge The Thailand Research Fund (TRF, BRG5680002), Department of Physics and Materials Science, Faculty of Science, Graduate School and Science and Technology Research Institute, Chiang Mai University, Thailand. The authors would like to acknowledge Department of Industrial Engineering, Faculty of Engineering, Rajamangala University of Technology Lanna (RMUTL), Thailand.

REFERENCES

1. Y. Tian, Y. Gong, D. Meng, Y. Li, and B. Kuang, *J. Electron. Mater.* 44, 2890 (2015).
2. Z. Yu, C. Ang, R. Guo, and A.S. Bhalla, *J. Appl. Phys.* 92, 2655 (2002).
3. P. Jarupoom, K. Pengpat, and G. Rujijanagul, *Curr. Appl. Phys.* 10, 557 (2010).
4. N. Lertcumfu, K. Pengpat, S. Eitssayeam, T. Tunkasiri, and G. Rujijanagul, *Ceram. Int.* 41, S447 (2015).
5. Z. Yu, C. Ang, R. Guo, and A.S. Bhalla, *Appl. Phys. Lett.* 81, 1285 (2002).
6. C. Kruea-In, S. Eitssayeam, K. Pengpat, T. Tunkasiri, and G. Rujijanagul, *Ferroelectric.* 145, 127 (2011).
7. P. Jarupoom and G. Rujijanagul, *J. Appl. Phys.* 114, 027018 (2013).
8. Q. Zhang, H. Sun, X. Wang, Y. Zhang, and X. Li, *J. Eur. Ceram. Soc.* 34, 1439 (2014).
9. P. Jarupoom, T. Tunkasiri, K. Pengpat, S. Eitssayeam, and G. Rujijanagul, *Ferroelectrics* 415, 88 (2011).
10. W. Eerenstein, N.D. Mathur, and J.F. Scott, *Nature* 442, 759 (2006).
11. Y. Chaudhari, C.M. Mahajan, A. Singh, P. Jagtap, R. Chatterjee, and S. Bendre, *J. Magn. Magn. Mater.* 395, 329 (2015).
12. K. Tang, W. Bai, J. Liu, J. Yang, Y. Zhang, C.G. Duan, X. Tang, and J. Chu, *Ceram. Int.* 41, S185 (2015).
13. K. Tajima, H.J. Hwang, M. Sando, and K. Niiihara, *J. Eur. Ceram. Soc.* 19, 1179 (1999).
14. H.J. Hwang, K. Tajima, M. Sando, M. Toriyama, and K. Niihara, *J. Ceram. Soc. Jpn.* 108, 339 (2000).
15. I. Fina, N. Dix, L. Fàbrega, F. Sánchez, and J. Fontcuberta, *Thin Solid Films* 518, 4634 (2010).
16. C. Kruea-In, T. Glansuvarn, S. Eitssayeam, K. Pengpat, and G. Rujijanagul, *Electron. Mater. Lett.* 9, 833 (2013).

17. N.S. Negi, A. Sharma, J. Shah, and R.K. Kotnala, *Mater. Chem. Phys.* 148, 1221 (2014).
18. J.L. Clabel, F.L. Zabotto, I.C. Nogueira, P. Schio, D. Garcia, O.F. de Lima, E.R. Leite, F.M.A. Moreira, and C.A. Cardoso, *J. Magn. Magn. Mater.* 364, 18 (2014).
19. P. Jarupoom, S. Eitssayeam, K. Pengpat, T. Tunkasiri, D.P. Cann, and G. Rujijanagul, *Nanoscale Res. Lett.* 7, 59 (2012).
20. K. Praveena and K.B.R. Varma, *J. Mater. Sci.: Mater. Electron.* 25, 5403 (2014).
21. J. Peng, M. Hojamberdiev, H. Li, D. Mao, Y. Zhao, P. Liu, J. Zhou, and G. Zhu, *J. Magn. Magn. Mater.* 378, 298 (2015).
22. P.S. Dobal, A. Dixit, R.S. Katiyar, Z. Yu, R. Guo, and A.S. Bhalla, *J. Appl. Phys.* 89, 8085 (2001).
23. S. Sen and R.N.P. Choudhary, *J. Mater. Sci.: Mater. Electron.* 15, 671 (2004).
24. L. Zhang, D. Xue, and C. Gao, *J. Magn. Magn. Mater.* 267, 111 (2003).
25. F. Moura, A.Z. Simoes, L.S. Cavalcante, M.A. Zaghete, J.A. Varela, and E. Longo, *J. Alloys Compd.* 466, L15 (2008).
26. L.S. Cavalcante, M. Anicete-Santos, J.C. Sczancoski, L.G.P. Simões, M.R.M.C. Santos, J.A. Varela, P.S. Pizani, and E. Longo, *J. Phys. Chem. Solids* 69, 1782 (2008).
27. N. Vittayakorn, S. Uttiya, G. Rujijanagul, and D.P Cann, *J. Phys. D: Appl. Phys.* 38, 2942 (2005).
28. A.S. Fawzi, A.D. Sheikh, and V.L. Mathe, *J. Alloys Compd.* 493, 601 (2010).
29. R.H. Kodama, S.A. Makhlouf, and A.E. Berkowitz, *Phys. Rev. Lett.* 79, 1393 (1997).
30. H. Yang, Y. Sun, Y. Lin, X. Zhang, X. Liu, T. Wang, and F. Wang, *J.Alloys Compd.* 695, 991 (2017).
31. X.Q. Chen, F.J. Yang, W.Q. Cao, H. Wang, C.P. Yang, D.Y. Wang, and K. Chen, *Solid State Commun.* 150, 1221 (2010).
32. H. Meštrić, R.A. Eichel, T. Kloss, K.P. Dinse, S. Laubach, St. Laubach, P.C. Schmidt, K.A. Schönau, M. Knapp, and H. Ehrenberg, *Phys. Rev. B* 71, 134109 (2005).
33. X. Chen, C. Wei, J. Xiao, Y. Xue, X. Zeng, F. Yang, P. Li, and Y. He, *J. Phys. D: Appl. Phys.* 46, 425001 (2013).
34. J.M.D. Coey, A.P. Douvalis, C.B. Fitzgerald, and M. Venkatesan, *Appl. Phys. Lett.* 84, 1332 (2004).
35. J. Rani, K.L. Yadav, and S. Prakash, *Mater. Res. Bull.* 60, 367 (2014).
36. X.L. Zhong, M. Liao, J.B. Wang, S.H. Xie, and Y.C. Zhou, *J. Cryst. Growth* 310, 2995 (2008).
37. T. Kimura, S. Kawamoto, I. Yamada, M. Azuma, M. Takano, and Y. Tokura, *Phys. Rev. B* 67, 180401(R) (2003).
38. N. Adhlakha, K.L. Yadav, and R. Singh, *J. Mater. Sci.* 50, 2073 (2015).
39. F. Moura, A.Z. Simões, B.D. Stojanovic, M.A. Zaghete, E. Longo, and J.A. Varela, *J. Alloys Compd.* 462, 129 (2008).
40. N. Nanakorn, P. Jalupoom, N. Vaneesorn, and A. Thanaboonsombut, *Ceram. Int.* 34, 779 (2008).
41. Z. Yu and C. Ang, *J. Appl. Phys.* 91, 794 (2002).
42. K. Pengpat, P. Jarupoom, P. Kantha, S. Eitssayeam, U. Intatha, G. Rujijanagul, and T. Tunkasiri, *Curr. Appl. Phys.* 8, 241 (2008).
43. C. Puchmark, G. Rujijanagul, S. Jiansirisomboon, T. Tunkasiri, N. Vittayakorn, T. Comyn, and S.J. Milne, *Curr. Appl. Phys.* 6, 323 (2006).
44. M. Sternitzke, *J. Eur. Ceram. Soc.* 17, 1061 (1997).
45. I. Ahmad, M. Islam, A.A. Almajid, B. Yazdani, and Y. Zhu, *Ceram. Int.* 40, 9327 (2014).
46. R.W. Rice, C.C. Wu, and F. Boichelt, *J. Am. Ceram. Soc.* 77, 2539 (1994).